

# Non-Equilibrium Ionization State and Two-Temperature Structure in the Bullet Cluster 1E0657-56

Takuya AKAHORI

Research Institute of Basic Science, Chungnam National University, Daejeon 305-764, Korea  
akataku@canopus.cnu.ac.kr

and

Kohji YOSHIKAWA

Center for Computational Sciences, University of Tsukuba, 1-1-1, Tennodai, Tsukuba, Ibaraki 305-8577  
kohji@ccs.tsukuba.ac.jp

(Received 2011 July 15; accepted 2011 September 3)

## Abstract

We investigate a non-equilibrium ionization state and an electron-ion two-temperature structure of the intracluster medium in the merging galaxy cluster, 1E0657-56 (the Bullet cluster), using a series of N-body and hydrodynamic simulations. We find that the electron temperature at the shock layer associated with the X-ray sub peak (bullet) is quite different depending on the thermal relaxation model between electrons and ions;  $\sim 25$  keV for the Coulomb thermal relaxation model and  $\sim 45$  keV for the instantaneous thermal relaxation model in the simulations which reproduce the observed X-ray morphology. Furthermore, both of Fe XXV and Fe XXVI are overabundant compared with the ionization equilibrium state around the shock layer, and thus, the intensity ratio between Fe XXV and Fe XXVI  $K\alpha$  lines are significantly altered from that in the ionization equilibrium state. We also carry out the simulations with various sets of merger parameters, and discuss a possible range of the non-equilibrium effects in this system. Our results could be tested with future X-ray observations such as *Astro-H* with better sensitivity in high energy band.

**Key words:** X-rays: galaxies: clusters — X-rays: individual (1E0657-56)

## 1. Introduction

Cosmological shock heating induced by successive merging of galaxies, galaxy groups, and clusters, are believed to be the main mechanism that have heated the X-ray emitting intracluster medium (ICM). Hydrodynamic simulations of the structure formation have shown that shock waves in galaxy clusters has a Mach number of a few in the standard  $\Lambda$ CDM cosmology (e.g., Ryu et al. 2003), which heat the ICM at most several tens keV. Such very hot ICM has been found through X-ray emission and the Sunyaev-Zel'dovich (SZ) effect (e.g., RXC J1347.5-1144: Kitayama et al. 2004; Ota et al. 2008, Abell 3667: Nakazawa et al. 2009), suggesting that violent mergers are ongoing in the context of a standard scenario of the hierarchical structure formation in the universe.

Cosmological shock waves are also important as laboratories of collisionless plasma. For instance, turbulent-flow motions induced via cascade of the vorticity generated at the shocks amplify magnetic fields through the turbulent dynamo (e.g., Ryu et al. 2008). Related to the magnetic field, particle acceleration and nonthermal emission are also interesting phenomena around the shocks (see Sarazin 2002 for a review). Distribution functions for shock heated electrons were recently studied in the framework of the relativistic correction of the SZ effect (Prokhorov et al. 2011a; Prokhorov et al. 2011b; Prokhorov et al. 2011c). In last decade, a possible difference in temperature between electrons

and ions, or the two-temperature structure, and the non-equilibrium ionization state of the ICM at the post-shock regions have been intensively investigated (Takizawa 1999; Takizawa 2000; Yoshida et al. 2005; Yoshikawa and Sasaki 2006; Cen, Fang 2006; Akahori and Yoshikawa 2008; Rudd, Nagai 2009; Akahori and Yoshikawa 2010; Wong et al. 2011).

Akahori and Yoshikawa (2010) (hereafter AY10) simulated merging galaxy clusters, relaxing the assumptions of both an ionization equilibrium and a thermal equipartition between electrons and ions, and found that both assumptions are not justified around the shocks in merging galaxy clusters, because their relaxation timescales, order of  $10^7$  yr for the electron density of  $10^{-3}$   $\text{cm}^{-3}$ , are not short enough compared with the merger timescale. They demonstrated that deviations from the ionization equilibrium and electron-ion equipartition states significantly affect an interpretation of the observational data such as the ICM temperature and metallicity. Therefore, studying the non-equilibrium effects is necessary not only to understand the relaxation mechanism in the plasma but also to correctly measure the properties of the shock-heated ICM with X-ray continuum emission of free electrons and X-ray line emissions of heavy elements. The effects of the non-equilibrium states in galaxy clusters have already been recognized with *Suzaku* X-ray observatory (Ota et al. 2008; Hoshino et al. 2010; Akamatsu et al. 2011).

1E0657-56 or RXC J0658.5-5556 ( $z = 0.296$ ) is known as one of the hottest galaxy clusters. It hosts an X-ray

sub peak on  $\sim 500$  kpc west side from a main peak in the *ROSAT* HRI image (Tucker et al. 1998). *Chandra* observations (Markevitch et al. 2002; Markevitch 2006) have revealed that the X-ray sub peak has a “bullet”-like shape, that is why 1E0657-56 is called the Bullet cluster. Except for a region around the sub peak, average ICM temperature was estimated to be  $kT = 17.4 \pm 2.5$  keV (Tucker et al. 1998) and  $14.1 \pm 0.2$  keV (Markevitch et al. 2002) from the fitting of the *ASCA* and *Chandra* data, respectively, which is relatively high compared with other observed clusters (e.g., Ota et al. 2006; Cavagnolo et al. 2009). Thermal SZ effect through such hot ICM was also observed (e.g., Zemcov et al. 2010). Optical-band observations have shown that galaxy components are clearly offset from the associated X-ray peaks (e.g., Barrena et al. 2002), and the gravitational potential does not trace the distribution of the ICM but follows approximately the distribution of galaxies as expected for a collisionless dark matter component (Clowe et al. 2004; Clowe et al. 2006; Bradač et al. 2006). These features suggest that a violent merger of a sub cluster is ongoing in the 1E0657-56 system. A density jump at a bow-shock structure ahead of the bullet indicates a shock front with a Mach number of  $M = 3.0 \pm 0.4$  (Markevitch 2006). Therefore, the 1E0657-56 system is a suitable target to investigate the non-equilibrium ionization state and the electron-ion two-temperature structure. Many theoretical works were devoted to numerical simulations of the 1E0657-56 system (Takizawa 2006; Milosavljević et al. 2007; Springel & Farrar 2007; Nusser 2008; Mastropietro & Burkert 2008), and concluded that an ongoing merger of two galaxy clusters can reproduce the observed features such as very hot ICM, shocks, and displacement between X-ray and column density peaks. These works, however, have assumed the ionization equilibrium of the ICM and the thermal equipartition between electrons and ions, and we are the first to address the non-equilibrium states of the ICM for further elucidation of the physical properties of the ICM in 1E0657-56 system.

In this paper, we investigate an ionization state and temperature structure of the ICM in the 1E0657-56 system, and clarify to what extent deviations from ionization equilibrium and thermal equipartition between electrons and ions arise and affect an interpretation of the observational data. We also discuss future prospects for the detectability of these non-equilibrium phenomena using the near future X-ray missions such as *Astro-H*.

The rest of this paper is organized as follows. In section 2, we describe the model and setup of the simulations. The results are shown in section 3. We discuss parameter dependence of our results and effect of radiative cooling in section 4 and 5, respectively, and summarize our conclusions in section 6. In the case that the cosmological scaling is required, we assume the density parameter,  $\Omega_M = 0.24$ , the cosmological constant,  $\Omega_\Lambda = 0.76$ , the baryon density parameter,  $\Omega_b = 0.04$ , and the Hubble constant,  $H_0 = 70$  km s $^{-1}$  Mpc $^{-1}$ , unless otherwise specified.

## 2. Numerical Simulation

We carry out a set of N-body and SPH simulations of the 1E0657-56 system, relaxing the assumptions of the ionization equilibrium of the ICM and the thermal equipartition between electrons and ions. Detailed descriptions of our simulation code were already published in AY10. Below, we briefly summarize our numerical schemes to treat the non-equilibrium ionization state and the thermal relaxation between electrons and ions as well as the setup of our simulations.

### 2.1. Electron-Ion Two Temperature Structure

Timescales on which each of electrons and ions achieves thermal relaxation through Coulomb scattering are much shorter than that between electrons and ions and a timescale of the merger in the cluster environment. Thus, we assume that electrons and ions always reach Maxwellian distributions with temperatures,  $T_e$  and  $T_i$ , respectively. Here, electrons and ions can have different temperatures just after experiencing shock heating, since most of the kinetic energy of the ICM is carried by ions at a shock front, and is preferentially converted to the thermal energy of ions in the post-shock regions (Fox, Loeb 1997). Afterward, thermal relaxation between electrons and ions proceeds toward the equipartition state.

Physical processes responsible for the thermal relaxation are still matter of debate. It is well known that the Coulomb scattering is not efficient enough to achieve electron-ion thermal equipartition in a timescale sufficiently shorter than typical merger timescale,  $\simeq 10^8$  yr, and it is argued that plasma waves are able to attain the thermal relaxation between electrons and ions more quickly than the Coulomb scattering. In this work, in order to bracket the plausible range of theoretical uncertainties regarding the thermal relaxation processes between electrons and ions, we present the results with two different thermal relaxation models: “single-temperature runs” in which the equipartition of thermal energy between electrons and ions is achieved instantaneously, and “two-temperature runs” which adopt only the Coulomb scattering as a physical process for thermal relaxation between electrons and ions.

In the two-temperature runs, we solve an ordinary energy equation for mixed fluid with a mean temperature,  $\bar{T} \equiv (n_e T_e + n_i T_i)/(n_e + n_i)$ , where  $n_e$  and  $n_i$  the number density of electrons and ions, respectively, and another equation for the time evolution of electrons which can be reduced to

$$\frac{d\tilde{T}_e}{dt} = \frac{\tilde{T}_i - \tilde{T}_e}{t_{ei}} - \frac{\tilde{T}_e}{u} Q_{sh}, \quad (1)$$

where  $\tilde{T}_e \equiv T_e/\bar{T}$  and  $\tilde{T}_i \equiv T_i/\bar{T}$  are the dimensionless temperatures of electrons and ions, respectively, normalized by the mean temperature,  $t_{ei}$  the Coulomb thermal relaxation timescale between electrons and ions (equation (3) of AY10), and  $u$  and  $Q_{sh}$  are the specific thermal energy and the shock heating rate per unit mass, respectively. We solve equation (1) in the same manner described in

Takizawa (1999).

The effect of radiative cooling of the ICM is considered in our simulations, in which only the thermal bremsstrahlung emission is considered since the ICM temperature is always high enough ( $\gg$  a few keV). We compute the cooling rate by using  $\bar{T}$  in the single-temperature runs and  $T_e$  in the two-temperature runs to incorporate the effect of two-temperature structure of the ICM consistently.

## 2.2. Non-Equilibrium Ionization State

The Lagrangian time evolution of ionization fractions of heavy elements, C, N, O, Ne, Mg, Si, S, and Fe, as well as hydrogen and helium is computed for each SPH particle by solving rate equations:

$$\frac{df_j}{dt} = \sum_{k=1}^{j-1} S_{j-k,k} f_k - \sum_{i=j+1}^{Z+1} S_{i-j,j} f_j - \alpha_j f_j + \alpha_{j+1} f_{j+1}, \quad (2)$$

where  $j$  is the index of a particular ionization stage considered,  $Z$  the atomic number,  $f_j$  the ionization fraction of an ion  $j$ ,  $S_{i,j}$  the ionization rate of an ion  $j$  with the ejection of  $i$  electrons, and  $\alpha_j$  is the recombination rate of an ion  $j$ . The ionization processes include collisional, Auger, charge-transfer, and photo-ionizations, and recombination processes are composed of radiative and dielectronic recombinations. We solve equation (2) in the same manner described in Yoshikawa and Sasaki (2006).

Ionization and recombination rates are calculated by utilizing the SPEX ver 1.10 software package<sup>1</sup>. In the two-temperature runs, the reaction rates are computed using the electron temperature,  $T_e$ , calculated from equation (1) in order to incorporate the effect of the two-temperature structure. As for the single-temperature runs, the reaction rates are computed using the mean temperature,  $\bar{T}$ . All ionization states of the atoms denoted above are considered in calculations of X-ray surface brightness. But in the following we only focus on the ionization state of iron, because most of ions except iron are fully-ionized for the ICM with the temperature higher than several keV in the 1E0657-56 system.

## 2.3. Simulation Setup

As an initial condition of the 1E0657-56 system, two spherically symmetric galaxy clusters are set up as follows. The virial radius,  $r_{200}$ , within which the mean mass density is 200 times the present cosmic critical density, and the virial mass,  $M_{200}$ , enclosed within  $r_{200}$  of a main (massive) cluster are set to  $r_{200} = 2.36$  Mpc and  $M_{200} = 1.5 \times 10^{15} M_{\odot}$ , respectively, and those of a sub (less massive) cluster are 1.21 Mpc and  $2.5 \times 10^{14} M_{\odot}$ , respectively. We adopt the hydrostatic model (AY10) with the NFW density profile (Navarro et al. 1997) for a dark matter halo, and the  $\beta$ -model density profile (Cavaliere & Fusco-Femiano 1976) with  $\beta = 2/3$  for an ICM component, and both of dark matter and SPH particles are initially distributed out to  $r_{200}$ . The scale radii,  $r_s$ , of the

NFW profile are set so that the concentration parameters  $c = r_s/r_{200} = 5$  and 8 for the main and sub clusters, respectively, and the core radius of the  $\beta$ -model is set to  $r_c = r_s/2$  for each cluster.

The main cluster is composed of  $10^7$  dark matter particles and the same number of SPH particles, while those of the sub clusters are proportional to their mass ratio. The corresponding spatial resolution of SPH is 12 kpc at the ICM density of  $10^{-2} \text{ cm}^{-3}$  (at the bullet) and 26 kpc at  $10^{-3} \text{ cm}^{-3}$  (at the shock front).

Our nominal run that reproduces the gross observed features of the 1E0657-56 system is organized as follows. Initially, two galaxy clusters contact each other at their outer edge,  $r_{200}$ . Their initial relative velocity is set to 3000 km/s, and the impact parameter is  $b = 0.236$  Mpc. Such an initial relative velocity and a non-zero impact parameter are required to reproduce a shock front with a Mach number of  $M \sim 3$  and asymmetric X-ray surface brightness (section 4; see also Mastropietro & Burkert 2008). As for the metallicity, a spatially uniform metallicity of 0.2 times solar abundance is assumed. In addition to that, we also assume  $\tilde{T}_e = \tilde{T}_i = 1$  and an ionization equilibrium state at the start of the simulations.

Compared with the previous hydrodynamic simulations (Springel & Farrar 2007; Mastropietro & Burkert 2008), the numbers of SPH and dark matter particles are  $\sim 5$ –10 times larger, so that the spatial resolution is roughly twice better. While Mastropietro & Burkert (2008) adopted the larger concentration parameters and smaller main cluster mass, we adopt the larger concentration parameters but the same main cluster mass as those adopted in Springel & Farrar (2007). This is because our parameters better reproduce the observed temperature profile at the pre-shock region in front of the bullet. While Springel & Farrar (2007) neglected the effect of radiative cooling, we demonstrate that considering radiative cooling is important since the radiative cooling significantly affects the width between the shock front and the contact discontinuity associated with “the bullet” (section 5). Although our nominal run reproduces an overall structure of the 1E0657-56 system well, as a practical interest, we also carried out the simulations with other sets of parameters, and discuss a possible range of the non-equilibrium effects (section 4).

## 3. Result

In the rest of this paper, we present the result after 1.12 Gyr has elapsed from the initial condition. At this epoch, the sub cluster already penetrates the center of the main cluster, and the separation between the centers of the main and sub clusters reaches  $\sim 0.72$  Mpc, which is consistent with that of the 1E0657-56 system (e.g., Clowe et al. 2004), assuming that the collision plane is perpendicular to the line-of-sight (the line-of-sight velocity difference of galaxies is estimated to be only 600 km/s; Barrena et al. 2002).

<sup>1</sup> (<http://www.sron.nl/divisions/hea/spex/>).

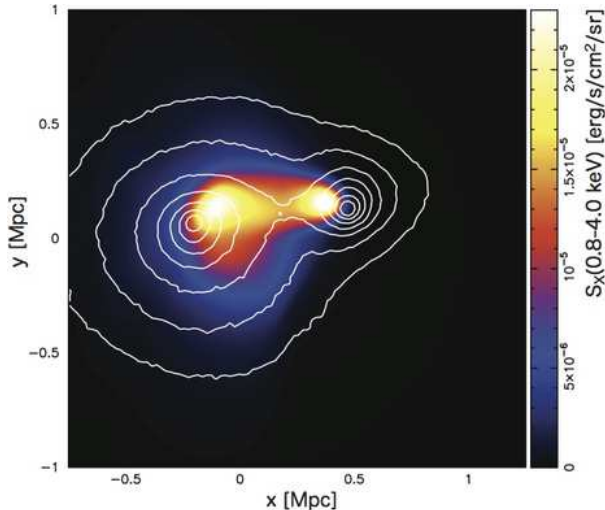


**Fig. 1.** X-ray surface brightness in the 0.8–4.0 keV band. The projected mass density (dark matter + ICM) is also overlaid (white contours). The core of the sub cluster (the right cluster) is moving from left to right hand side and has already penetrated the main cluster (the left cluster).

### 3.1. Overall Structure of Simulated 1E0657-56

We first present the overall structure of the simulated clusters in order to make sure that our simulation reproduces the gross observed features of the 1E0657-56 system, and to locate the regions where the effects of the non-equilibrium ionization state and the two-temperature structure remarkably take place.

Figure 1 depicts the 0.8–4.0 keV band X-ray surface brightness map and the contours of the projected mass density (dark matter + ICM) integrated along the line-of-sight. Our nominal run nicely reproduces the overall structure of the 1E0657-56; for instance, distinct two X-ray peaks, positions and shapes of shock front and contact discontinuity, and displacement between X-ray and projected mass density peaks associated with the sub cluster, are consistent with the observations (Markevitch 2006; Clowe et al. 2004).

Figure 2 shows the temperature maps on the collision plane of the two galaxy clusters. There exists very hot ICM heated from  $\sim 8$  keV to more than  $\sim 30$  keV by a shock wave with a Mach number of  $M \sim 2-3$  in front (the right hand side) of the cold core (the bullet) of the sub cluster. The shock layer extends toward the outskirts of the clusters, which has a Mach number of  $M \sim 1.5-2.5$  and heats the ICM to  $\sim 15-20$  keV. In the two-temperature run, we can see that the electron temperature is typically  $\sim 30-50$  % lower than the mean temperature behind the shock (the bottom panel of figure 2). The two-temperature structure can not be seen inside the bullet, because the timescale of thermal relaxation between electrons and ions are much shorter than the merger timescale due to the high density and low temperature. We have another high temperature region behind the bullet heated by the compressive flows.

Figures 3 and 4 show the ratios of Fe XXV and Fe XXVI

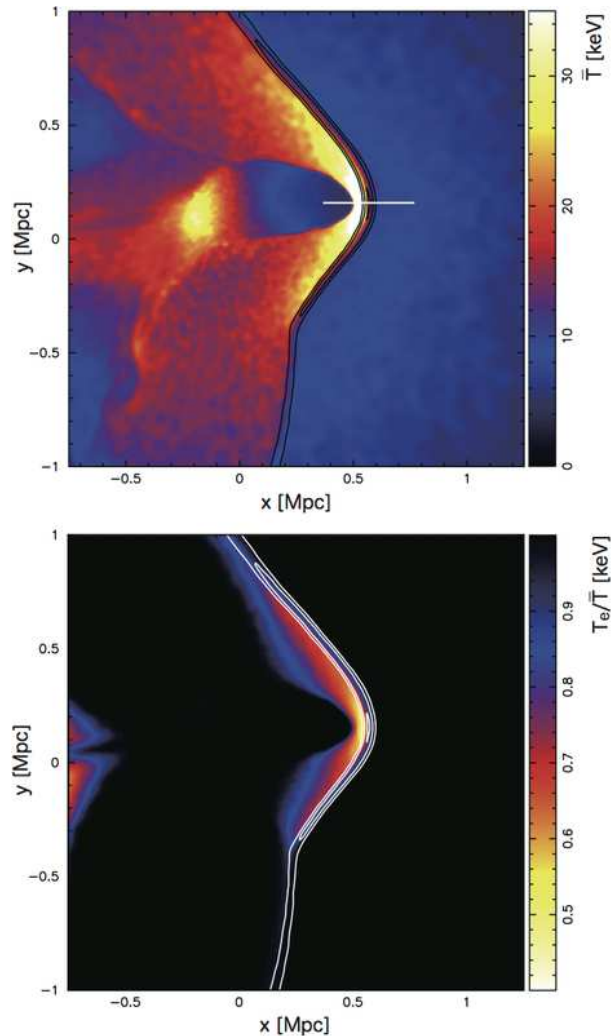


**Fig. 2.** The mean temperature of ICM,  $\bar{T}$ , (top) and the ratio of the electron temperature relative to the mean temperature,  $T_e/\bar{T}$ , (bottom), on the collision plane of the two galaxy clusters. Contours show the Mach number on the collision plane from 1.5 by 0.5, and the innermost contour represents the Mach number of 2.5, estimated by the shock-capture method described in Pfrommer et al. (2006). A white horizontal line indicates the location of the one-dimensional profile discussed in figure 7.

fractions relative to those in the ionization equilibrium state, respectively. Here, in the two-temperature run, ionization fractions in the ionization equilibrium state are computed using the mean temperature. We find that both Fe XXV and Fe XXVI are overabundant by 1.2–3.0 behind the shock layer, and the deviations from the equilibrium value are larger in the two-temperature run. The overpopulation of Fe XXV and Fe XXVI fractions can be understood as follows. The shock heats the ICM in the post-shock region from several keV to a few tens keV, and both of Fe XXV and Fe XXVI fractions in the post-shock region decrease with time toward the equilibrium value because their fractions are maximized at  $\sim 3$  keV and  $\sim 10$  keV, respectively, in the ionization equilibrium state (see figure 4 of AY10). However, the ionization of Fe XXV and Fe XXVI



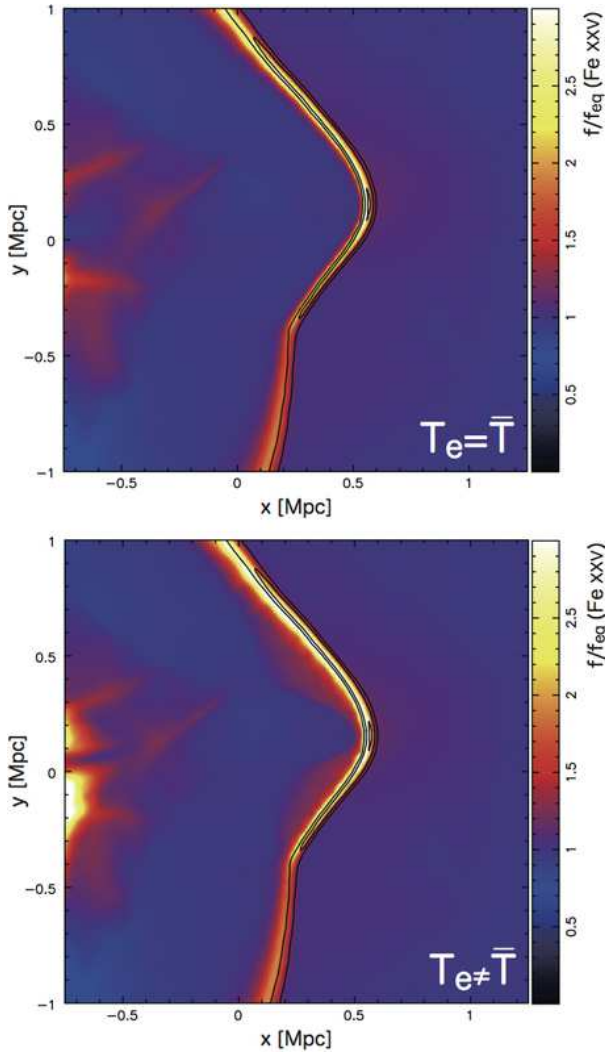


**Fig. 3.** The ratio of the ionization fraction of Fe XXV relative to that in the ionization equilibrium state on the collision plane of the two galaxy clusters. Top and bottom panels show the results of the single- and two-temperature runs, respectively. Black contours are the same as figure 2.

toward higher-ionized levels is not quick enough to catch up with the ionization equilibrium state. Therefore, these fractions are higher than that in the ionization equilibrium state. Since the ionization rates of ions to the higher ionization levels depend on the electron temperature, and the rates are significantly smaller in the two-temperature run, a delay of the heating of electrons at the shock leaves these fractions higher than that in the single-temperature run.

To see an observational appearance of the result of the nominal runs, we calculate the spectroscopic-like temperature ( $T_{sl}$ , Mazzotta et al. 2004) and the ratio,  $R/R_{eq}$ , as an observational tracer for the non-equilibrium ionization state (AY10), where  $R$  is the X-ray intensity ratio between rest-frame 6.6–6.7 keV and 6.9–7.0 keV energy bands in which the Fe XXV  $K\alpha$  and Fe XXVI  $K\alpha$  emissions are predominant, respectively;

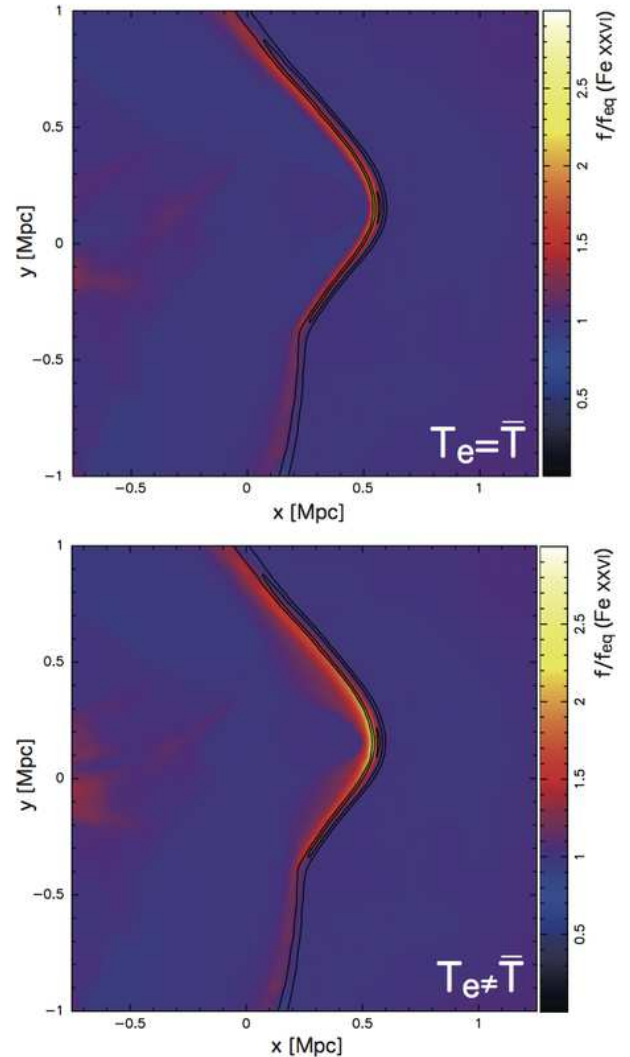


**Fig. 4.** Same as figure 3 but for the ionization fraction of Fe XXVI.

$$R = \frac{I(6.6 - 6.7 \text{ keV})}{I(6.9 - 7.0 \text{ keV})}, \quad (3)$$

and  $R_{eq}$  is the intensity ratio defined above but in the ionization equilibrium state. It should be noted that the quantity,  $R/R_{eq}$ , is independent on the ICM metallicity. The results are shown in figures 5 and 6. In terms of the spectroscopic-like temperature, the temperature of the ICM at the shock in front of the bullet is roughly  $\sim 15$  keV in the two-temperature run, and lower than in the single-temperature run.  $R/R_{eq}$  departs from unity ( $\sim 1.1$ – $1.2$ ) both in the single- and two temperature runs, though its difference between the two runs is not significant. In both single- and two-temperature runs, the deviation of the intensity ratio is more significant in the outskirts than in the central part of the clusters, since the timescale to reach the ionization equilibrium state is longer in the lower-density regions.

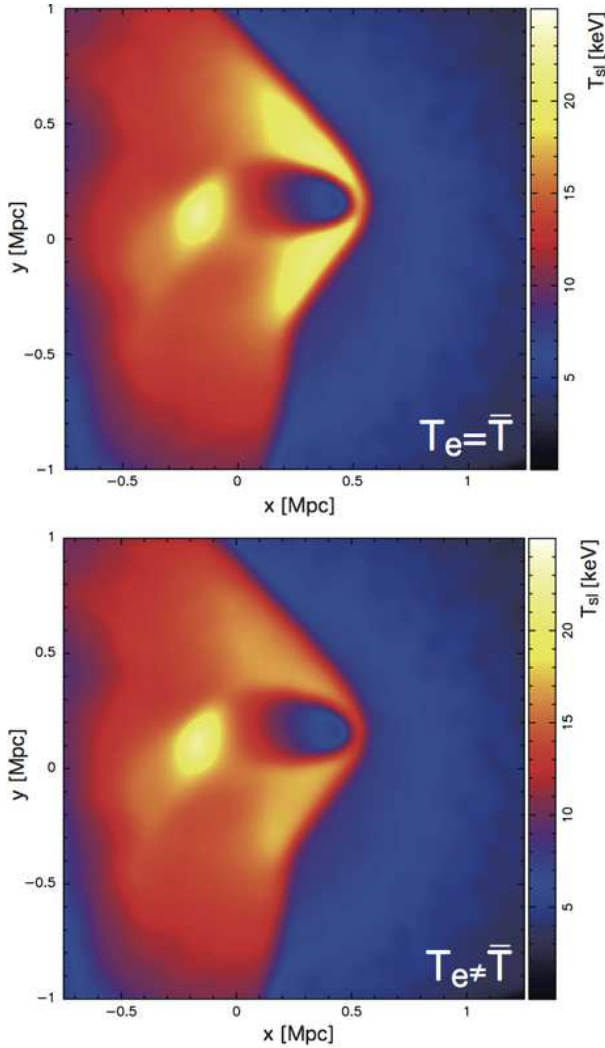


**Fig. 5.** The spectroscopic-like temperature (Mazzotta et al. 2004). Top and bottom panels show the results of the single- and two-temperature runs, respectively.

### 3.2. Detailed Structures of Bullet and Shock

The shock front ahead of the bullet is suited to the study of the non-equilibrium ionization state and the two-temperature structure of the ICM, since the strong shock with a Mach number of  $3.0 \pm 0.4$  is reported (Markevitch 2006) and the observational signatures of the departure from the ionization equilibrium and the two-temperature structure are expected to be relatively strong. In this subsection, we present the detailed analyses of the shock ahead of the bullet, and how such observational signatures can be detected in X-ray observations.

Figure 7 shows the one dimensional profiles of the ICM across the bullet and the shock front on a line on the collision plane, the location of which is indicated by a white line in figure 2. We can see that the shock velocity, the relative velocity of the ICM between pre- and post-shock regions, is about 5000 km/s (figure 7(b)), which is consistent with the previous simulations (Takizawa 2006; Milosavljević et al. 2007; Springel

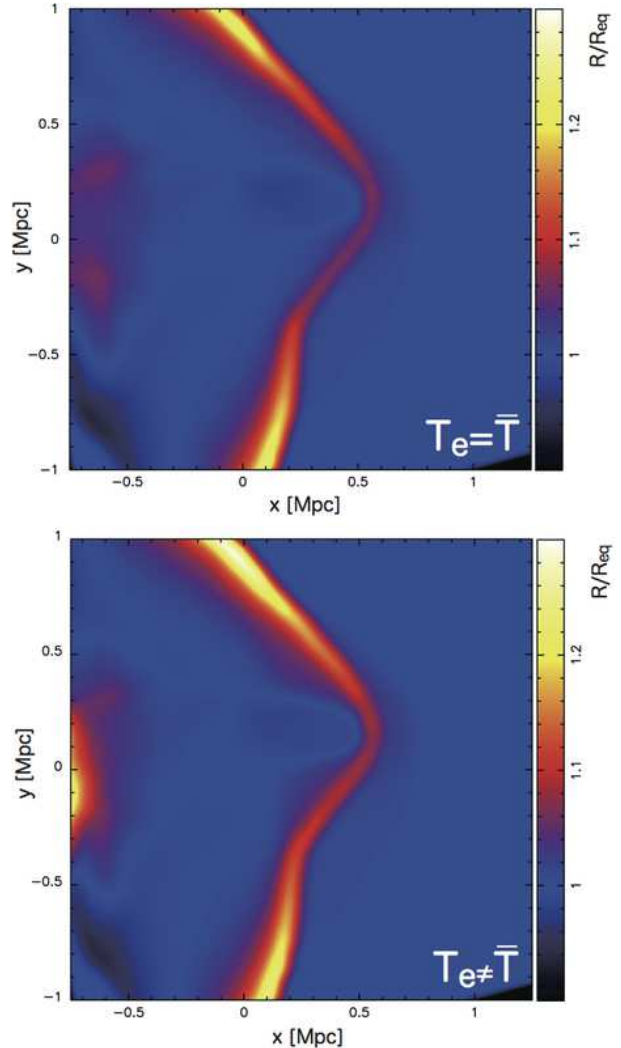


**Fig. 6.**  $R/R_{eq}$  (see equation (3)). Top and bottom panels show the results of the single- and two-temperature runs, respectively.

& Farrar 2007; Mastrogiro & Burkert 2008), The Mach number of the shock is  $\sim 2.8$ , and consistent with the estimate based on X-ray observations by *Chandra* (Markevitch 2006).

In the two-temperature run, we find that the electron temperature between the shock front and the contact discontinuity is  $T_e \sim 25$  keV and much lower than the mean temperature,  $\bar{T} \sim 45$  keV. In the single-temperature run, the temperature of the ICM is almost the same as the mean temperature in the two-temperature run, and the profiles of the ICM density and velocity are also unchanged regardless of the thermal relaxation model adopted. This means that the difference in the cooling rate due to the difference in the electron temperature does not affect the overall hydrodynamic properties of the ICM.

We can see that the ionization state of iron strongly deviates from the ionization equilibrium state between the shock front and the contact discontinuity, and the ratios of FeXXV and FeXXVI fractions relative to those in the

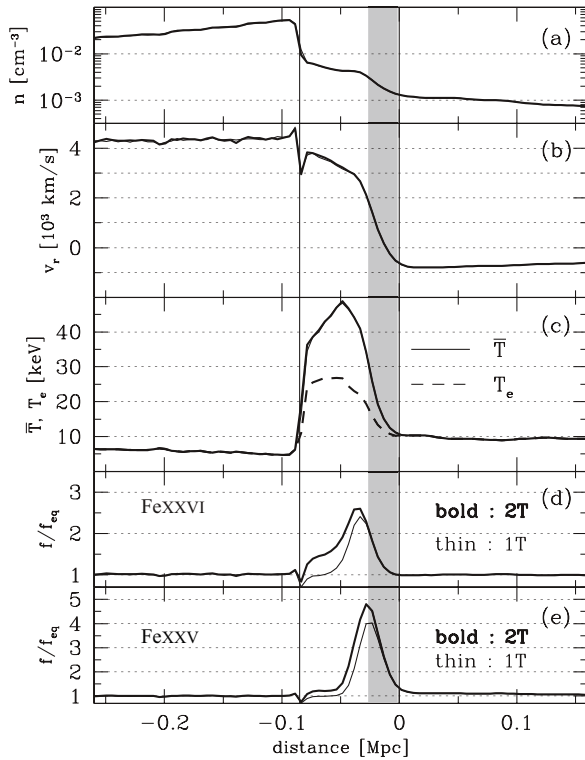


**Fig. 7.** One dimensional profiles across the shock front on the collision plane. Thin and thick lines show the results of the single- and two-temperature runs, respectively. Panels from the top to the bottom show (a) the ICM density, (b) the ICM velocity along the axis, (c) the average temperature (solid line) and the electron temperatures in the two-temperature run (dashed line), (d) the ratio of ionization fractions of FeXXVI relative to that in the ionization equilibrium state, and (e) the ratio for FeXXV. Two vertical lines indicate the location of the shock front (right) and the contact discontinuity (left). The coordinate of the horizontal axis shows the distance measured from the shock front.

ionization equilibrium state reach  $\sim 5$  and  $\sim 2.5$ , respectively (figures 7(d) and 7(e)). The amount of the departure from the ionization equilibrium state depends on the adopted thermal relaxation model and larger in the two-temperature run.

Figure 8 shows the profiles of X-ray surface brightness in the 0.8–4.0 keV band (panel (a)), spectroscopic-like temperature (panel (b)), and  $R/R_{\text{eq}}$  (panel (c)) projected along the line-of-sight at the same region as figure 7. In these projected quantities, the signatures of the two-temperature structure and the non-equilibrium ionization state are contaminated by the contributions of the foreground and background ICM. Nevertheless, we can see such signatures in figure 8 to some extent. In the two-temperature run, the maximum spectroscopic-like temperature between the shock front and the contact discontinuity is  $\sim 20$  keV and significantly lower than that in the single-temperature run ( $\sim 25$  keV).  $R/R_{\text{eq}}$  also deviates from unity at the same region, indicating the non-equilibrium ionization state in this region, though the dif-

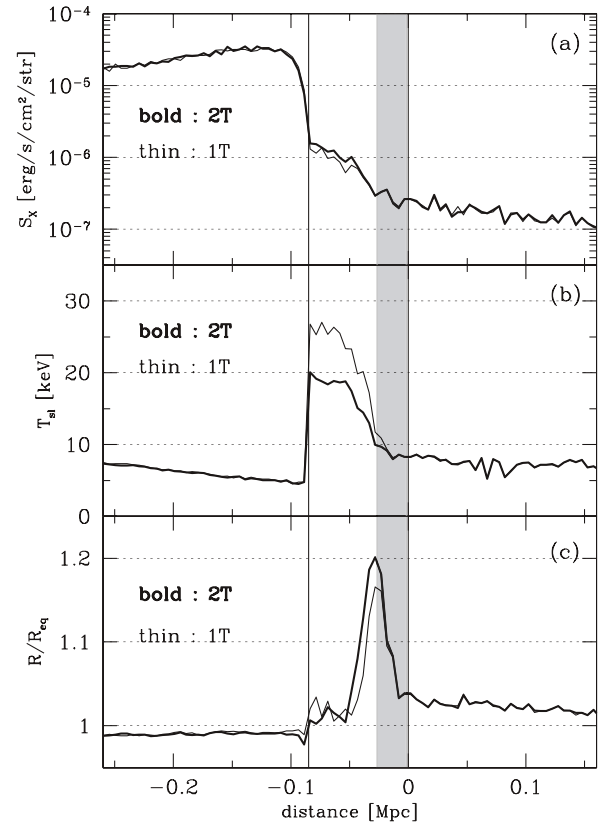


**Fig. 8.** Same as figure 7 except that panels from the top to the bottom show (a) the surface brightness in the 0.8–4.0 keV energy band, (b) the spectroscopic-like temperature, and (c)  $R/R_{\text{eq}}$  projected along the line-of-sight, respectively.

ference between the single- and two-temperature runs is not significant.

It should be noted that, due to the poor capability of the SPH scheme to resolve the shock front, the discontinuities of physical quantities such as density and temperature across the shock front are numerically smeared in our simulations, and that the actual jumps of density, velocity and temperature of the ICM should be sharper in “reality”. The shaded regions in figures 7 and 8 indicate the locations where such numerical smearing is effective. If the jumps of physical quantities at the shock are ideally resolved, it is expected that the difference in temperature between electrons and ions at the post-shock regions and the departure from the ionization equilibrium state are larger at the post-shock region. Therefore, the difference of projected profiles of the spectroscopic-like temperature between the single- and two-temperature runs would be larger, and thus the difference of  $R/R_{\text{eq}}$  between the single- and two-temperature runs would be also more significant.

#### 4. Dependence on the Initial Condition

In this section, in order to figure out parameter dependence of our results, we compare various merger simulations with different sets of parameters.

First, we briefly summarize morphological differences of the simulated clusters. The followings are notable dependences on the initial parameters that we confirmed:

- An overall structure of the observed features such as the bullet, the shock layer, and the peaks of X-ray surface brightness and projected mass density are best reproduced with the concentration parameter,  $c = 5$ , of the main cluster. The runs with  $c = 3$  (e.g., Springel & Farrar 2007) give similar results, but produce X-ray and projected mass density maps of the main cluster slightly more elongated along north-south direction. Difference in the simulations with  $c = 5$  and those with  $c = 6$  adopted by Mastropietro & Burkert (2008) is almost negligible.
- The displacement between the peaks of X-ray surface brightness and projected mass density in the sub cluster (the bullet) are best reproduced with the concentration parameter,  $c = 8$ , of the sub cluster (Mastropietro & Burkert 2008). For  $c > 8$ , the bullet gets close to the projected density peak, and the displacement becomes smaller.
- As pointed out by Mastropietro & Burkert (2008), a non-zero impact parameter is necessary to reproduce the asymmetric X-ray surface brightness. However, the runs in which the sub-cluster gets through the south side of the main cluster can not simultaneously reproduce the observed X-ray surface brightness and projected mass density. Therefore, we adopt the sub-cluster’s orbit which passes through the north side of the main cluster.
- The initial relative velocity of 3000 km/s is required to reproduce the shock layer with a Mach number of  $M \sim 3$  in front of the bullet. Similar requirement has been also indicated in other numerical studies on the bullet cluster (Takizawa 2006; Milosavljević et al. 2007; Springel & Farrar 2007; Mastropietro & Burkert 2008). According to Hayashi, White (2006), an encounter with the virial velocity of the main cluster,  $V_{200} \sim 1700$  km/s, and the relative velocity,  $V_{\text{sub}} \sim 3000$  km/s, is probable with a relative likelihood of  $f \sim 0.03$ , based on the cosmological structure formation simulations (see equation (1) of Hayashi & White 2006, where we adopted  $v_{10\text{percent}} = 1.55$ , and  $\alpha = 3.3$ ). However, it should be noted that the probability for such a high initial relative velocity is still controversial: Lee, Komatsu (2010) recently claimed that the initial relative velocity of 3000 km/s at  $R_{200}$  is very unusual with the prediction of the concordance  $\Lambda$ CDM model. Even if we admit a  $M \sim 2.5$  shock as the lower limit of the observed Mach number, the required initial relative velocity is  $\sim 2500$  km/s, and is still peculiarly high.

- The contrast of the peak brightness relative to that of the ambient gas is best reproduced with the initial mass ratio of 6 : 1 between the main and the sub clusters. With decreasing the mass ratio, the X-ray peak of the main cluster becomes dimmer (see e.g., 3 : 1 runs of Mastropietro & Burkert 2008). Note that the mass ratio also affects the Mach number of the shock; the run with the mass ratio of 4 : 1 produces the shock with the Mach number larger than 3 for the initial relative velocity of 3000 km/s, and allows us to adopt smaller initial relative velocity to reproduce the  $M \sim 3$  shock.

Using the various merger simulations with different sets of parameters, let us evaluate a possible range of the non-equilibrium effects in the 1E0657-56 system. Based on the simulations in this and previous works (Springel & Farrar 2007, Mastropietro & Burkert 2008), we consider the results with the initial mass ratio, 4 : 1, 6 : 1, or 10 : 1, and the concentration parameter  $c = 3$  or 5 for the main cluster and 8 or 10 for the sub cluster, which are consistent with the observational features of the 1E0657-56 system to some extent. To identify the snapshot that corresponds to the “current” epoch in the time sequences of the simulations, we adopt the separation of two peaks of the projected mass density. The other parameters such as the mass of the main cluster and the impact parameter are the same as our nominal run except that we use one eighth of the number of particles (the smoothing length is thus twice as large). We adopt the same initial relative velocity of 3000 km/s regardless of the mass ratio, since, in our prescription to determine the initial relative velocity described in Sarazin (2002), it is proportional to the square root of the mass ratio and has weak dependence on the mass ratio.

In table 1, we present the physical properties of the shock front associated with the bullet for the runs with the simulation parameters different from our nominal run. We find that  $R/R_{\text{eq}} = 1.1\text{--}1.4$  in the two-temperature runs, with the Mach number ranging from  $M = 2.5$  to 3.4. We also find that  $\bar{T} = 33\text{--}50$  keV and  $T_e = 9\text{--}24$  keV, or  $T_e/\bar{T} = 0.2\text{--}0.7$ . In other words, the observed electron temperature at the shock lower than  $\sim 25$  keV suggests that the Coulomb collision is a predominant process of thermal relaxation between electrons and ions and that there exists the two-temperature structure at the shock front. On the other hand, the observed electron temperature higher than  $\sim 30$  keV prefer the instantaneous thermal relaxation at the shock front.

The *Chandra* observation suggests that the deprojected electron temperature behind the shock is over  $\sim 30$  keV (Markevitch 2006), which is higher than the constraint for the existence of the two-temperature structure we obtained in the two-temperature runs. This suggests that, although there are still uncertainties due to the spatial resolution in both observations and simulations, the instantaneous thermal relaxation model is preferable for reproducing the observed temperature structure at the shock. Markevitch (2006) discussed that the simple model of



**Table 1.** Physical properties of the shock in front of the bullet for the runs “cXcYmZ” where X and Y denotes the concentration parameters of the main and sub clusters, respectively, and the mass ratio of the two clusters is Z : 1.  $\bar{T}$  and  $T_e$  are in units of keV.

run ID	$M$	$\bar{T}$	$T_e$	$T_e/\bar{T}$	$R/R_{\text{eq}}$
c03c08m04	3.0	44	21	0.47	1.25
c03c08m06	3.0	43	21	0.50	1.26
c03c08m10	2.6	33	20	0.62	1.24
c03c10m04	3.1	49	20	0.40	1.29
c03c10m06	3.4	41	13	0.31	1.36
c03c10m10	3.2	34	8.3	0.26	1.19
c05c08m04	2.9	47	24	0.51	1.27
c05c08m06	3.0	43	23	0.54	1.19
c05c08m10	2.5	34	22	0.65	1.18
c05c10m04	3.1	50	22	0.43	1.23
c05c10m06	3.0	49	16	0.34	1.14
c05c10m10	3.2	42	9.9	0.23	1.16

electron-ion thermal relaxation only through the Coulomb scattering is inconsistent with the observed data and is excluded at a 95% confidence level, implying that the thermal equilibration between electrons and ions should be much faster than that by the Coulomb scattering. We, however, should notice that the accuracy of the observed electron temperature by *Chandra* is somewhat limited in the high energy band more than  $\sim 10$  keV. Thus, this issue should be addressed by the observations with future X-ray satellites such as *Astro-H* with better sensitivity in high energy band. Another plausible way to measure the temperature of very hot ICM should be a joint analysis with the X-ray and SZ data (Kitayama et al. 2004). The analysis of the Bullet cluster that is based on the high-resolution X-ray and SZ observations such as *Chandra* and *Herschel-SPIRE* will provide us new constraints on very hot thermal and/or non-thermal particle populations (Prokhorov, Akahori, Yoshikawa, et al., in preparation).

## 5. Effect of Radiative Cooling

Finally, we discuss the effect of radiative cooling on the properties of the simulated bullet clusters.

As partly discussed in section 3.2, the thermal relaxation model does not significantly change the overall hydrodynamic properties of the ICM. This is because the radiative cooling is inefficient in the pre-shock region and the shock layer, where radiative cooling timescale is longer than the age of the universe, regardless of the difference in the cooling rate due to the difference in the electron temperature. As for the bullet, radiative cooling is efficient, but there are no two-temperature structure due to a short relaxation timescale between electrons and ions, so that the effect of radiative cooling is identical there. Therefore, morphology of the X-ray surface brightness does not de-

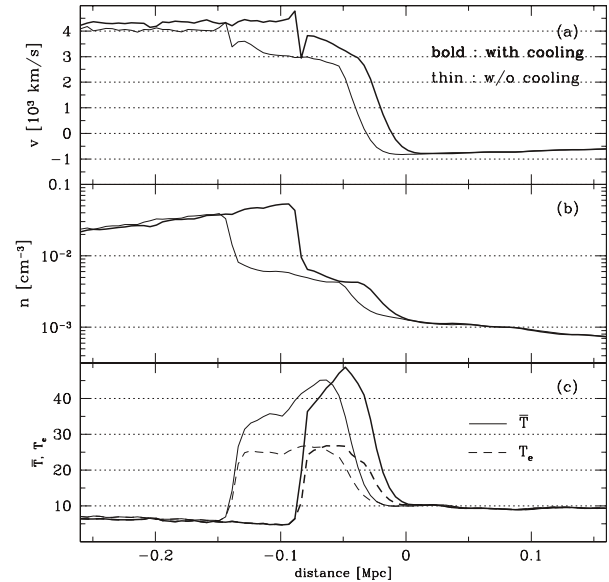


**Fig. 9.** One dimensional profiles across the bullet and the shock on the collision plane for the two-temperature runs. Thin and thick lines show the results of the non-cooling and cooling runs, respectively. Panels from the top to the bottom shows (a) the ICM velocity along the axis, (b) the ICM density, and (c) the average temperature (solid) and the electron temperature (dashed).

pend significantly on the thermal relaxation model, and thus we basically obtain the same best fit parameters for different thermal relaxation model.

Considering the effect of radiative cooling is, however, quite important to determine the location of the bullet in the 1E0657-56 system. In order to demonstrate the effect, we carried out the control run in which we neglect the effect of radiative cooling, and compared it with the cooling run that we have shown. The results after 1.12 Gyr has elapsed for the two-temperature runs are shown in figure 9, where the axes of the profile for two runs are the same as that shown in figure 2. We can see a delay of the propagation of the bullet and the shock in the non-cooling run. Moreover, the width between the shock front and the contact discontinuity becomes wider in the non-cooling run than that in the cooling run. This may be ascribed to the fact that the gravitational binding force is weaker, i.e. ram pressure becomes more significant, in the non-cooling run, since the bullet less concentrates compared with the cooling run (by a factor of  $\sim 1.6$  at the present). Our result suggests that considering the effect of radiative cooling is important to correctly constrain the initial relative velocity from the measurement of the width between the shock front and the contact discontinuity (Mastropietro & Burkert 2008).

## 6. Summary and Conclusion

We conduct a set of  $N$ -body/SPH simulations of merging galaxy clusters which reproduce observed X-ray sur-

face brightness and projected mass density distribution of the 1E0657-56 system to investigate the non-equilibrium ionization state and electron-ion two-temperature structure in the 1E0657-56 system, and to assess their detectability in future X-ray missions. Different from previous numerical works of the 1E0657-56 system, we, for the first time, relax the both assumptions of ionization equilibrium and thermal equipartition between electrons and ions.

Our nominal run, which reproduces the various observed features of the 1E0657-56 system fairly well, is an merger of two galaxy clusters with a mass ratio of 6:1 and an initial relative velocity of 3000 km/s. It is found that departure from the ionization equilibrium is significant at the shock front with a Mach number of  $M \sim 3$  associated with the penetrating core of the sub cluster. When considering only the Coulomb scattering as a physical process for the thermal relaxation between electrons and ions, we find that the two-temperature structure, or the difference in temperature between electrons and ions, are also significant at the shock front.

Comparisons of the X-ray and column density profiles with those in the observations gave possible range of simulation parameters. Within the range, at the shock associated with the bullet we found that  $R/R_{\text{eq}}$  (equation (3)) clearly deviates from unity and the electron temperature is much lower than the mean temperature of the ICM in the two-temperature run. Effect of radiative cooling is important to determine the location of the bullet, where the overall hydrodynamic properties of the ICM is not significantly altered by the different efficiency of radiative cooling due to the different temperature structure.

It is found that, in the two-temperature run, the spectroscopic-like temperature projected along the line-of-sight between the shock front and the contact discontinuity is significantly lower than that in the single-temperature run, which suggests that precise measurements of the maximum electron temperature in this region could provide strong constraints on thermal relaxation processes between electrons and ions. Such observations can be available with a high sensitivity X-ray detector in high energy band and also with a good spatial resolution to resolve the relatively tiny area between the shock front and the contact discontinuity. Observations of thermal Sunyaev–Zel’dovich effect with relatively good spatial resolution can provide an independent measurement of electron temperature in this region. A good spectroscopic resolution in X-ray observations is also important in studying the two-temperature structure of the ICM, because the ion temperature is only estimated from the detailed line profiles of emission lines, and would be achieved by X-ray calorimeters on board the forthcoming satellites. Our results also suggest that the current X-ray observations can lead to a biased result on the estimation of the metallicity if one assumes that the ICM is in the ionization equilibrium state, because the separate detection of emission lines of Fe XXV and Fe XXVI is still difficult with the current X-ray observational facilities due to a lack of the spectroscopic resolution of the CCDs. Therefore, a

good spectroscopic resolution is also needed to correctly measure the metallicity in the shock heated ICM.

This work was supported in part by Grant-in-Aid for Scientific Research (S) (20224002), for Scientific Research (A) (20340041), for Young Scientists (Start-up) (19840008) and for Challenging Exploratory Research (21654026) from JSPS. Numerical simulations for the present work had been carried out under the “Interdisciplinary Computational Science Program” in Center for Computational Sciences, University of Tsukuba. TA was supported in part by Korea Science and Engineering Foundation (R01-2007-000-20196-0) and by the National Research Foundation of Korea (2007-0093860).

## References

- Akahori, T., & Yoshikawa, K. 2008, PASJ, 60, L19  
 Akahori, T., & Yoshikawa, K. 2010, PASJ, 62, 335  
 Akamatsu, H., Hoshino, A., Ishisaki, Y., Ohashi, T., Sato, K., Takei, Y., & Ota, N. 2011, PASJ, in press (arXiv:1106.5653)  
 Barrena, R., Biviano, A., Ramella, M., Falco, E. E., & Seitz, S. 2002, A&A, 386, 816  
 Bradač, M. et al. 2006, ApJ, 652, 937  
 Cavaliere, A., & Fusco-Femiano, R. 1976, A&A, 49, 137  
 Cavagnolo, K. W., Donahue, M., Voit, G. M., & Sun, M. 2009, ApJS, 182, 12  
 Cen, R., & Fang, T. 2006, ApJ, 650, 573  
 Clowe, D. Gonzalez, A., & Markevitch, M. 2004, ApJ, 604, 596  
 Clowe, D. Bradač, M., Gonzalez, A. H., Markevitch M., Randall, S. M., Jones, C., & Zaritsky D. 2006, ApJ, 648, L109  
 Fox, D. C., & Loeb, A. 1997, ApJ, 491, 459  
 Hayashi, E., & White, S. D. M. 2006, MNRAS, 370, L38  
 Hoshino, A., et al. 2010, PASJ, 62, 371  
 Kitayama, T., Komatsu, E., Ota, N., Kuwabara, T., Suto, Y., Yoshikawa, K., Hattori, M., & Matsuo, H. 2004, PASJ, 56, 17  
 Lee, J., & Komatsu, E. 2010, ApJ, 718, L60  
 Markevitch, M., Gonzalez, A. H., David, L., Vikhlinin, A., Murray, S., Forman, W., Jones, C., & Tucker, W. 2002, ApJ, 567, L27  
 Markevitch, M. 2006, in Willson A., ed., Proc. The X-ray Universe 2005, ESA Publ. Div., Noordwijk, p. 723  
 Mastroiello, C., & Burkert, A. 2008, MNRAS, 389, 967  
 Mazzotta, P., Rasia, E., Moscardini, L., & Tormen, G. 2004, MNRAS, 354, 10  
 Milosavljević, M., Koda, J., Nagai, D., Naker, E., & Shapiro, P. R. 2007, ApJ, 661, L131  
 Nakazawa, K., et al. 2009, PASJ, 61, 339  
 Navarro, F. J., Frenk, C. S., & White, S. D. M. 1997, ApJ, 490, 493  
 Nusser, A. 2008, MNRAS, 384, 343  
 Ota, N., Kitayama, T., Masai, K. & Mitsuda, K. 2006, ApJ, 640, 673  
 Ota, N., Murase, K., Kitayama, T., Komatsu, E., Hattori, M., Matsuo, H., Oshima, T., Suto, Y. & Yoshikawa, K. 2008, A&A, 491, 363  
 Pfrommer, C., Springel, V., Enßlin, T. A., & Jubelgas, M. 2006, MNRAS, 367, 113

- Prokhorov, D. A., Colafrancesco, S., Akahori, T., Yoshikawa, K., Nagataki, S., & Seon, K. I. 2011a, *A&A*, 529, 39
- Prokhorov, D. A., Dubios, Y., Nagataki, S., Akahori, T., & Yoshikawa, K. 2011b, *MNRAS*, in press (arXiv:1104.2357)
- Prokhorov, D. A., Colafrancesco, S., Akahori, T., Million, E. T., Nagataki, S., & Yoshikawa, K. 2011c, *MNRAS*, in press (arXiv:1105.4271)
- Rudd, D. H., & Nagai, D. 2009, *ApJL*, 701, L16
- Ryu, D., Kang, H., Hallman, E., & Jones, T. W. 2003, *ApJ*, 593, 599
- Ryu, D., Kang, H., Cho, J., & Das, S. 2008, *Science*, 320, 909
- Sarazin, C. 2002, *Merging Processes in Clusters of Galaxies*, ed. Feretti, L., Gioia, I. M., & Giovannini, G. (Dordrecht: Kluwer Academic Publishers), *Astrophysics and Space Science Library*, 272, 1
- Springel, V., & Farrar, G. 2007, *MNRAS*, 380, 911
- Takizawa, M. 1999, *ApJ*, 520, 514
- Takizawa, M. 2000, *ApJ*, 532, 183
- Takizawa, M. 2006, *PASJ*, 58, 925
- Tucker, W., Blanco, P., Rappoport, S., David, L., Fabricant, D., Falco, E. E. Forman, W., Dressler, A., & Ramella, M. 1998, *ApJ*, 496, L5
- Wong, K. W., Sarazin, C., & Ji, L. 2011, *ApJ*, 727, 126
- Yoshikawa, K., & Sasaki, S. 2006, *PASJ*, 58, 641
- Yoshida, N., Furlanetto, S. R., & Hernquist, L. 2005, *ApJ*, 618, L91
- Zemcov, M. et al. 2010, *A&A*, 518, L16